

Fine-grained Image Aesthetic Assessment: Learning Discriminative Scores from Relative Ranks

Zhichao Yang^{1†}, Jianjie Wang^{1†}, Zhixianhe Zhang¹, Pangu Xie¹, Xiangfei Sheng¹,
Pengfei Chen¹, and Leida Li^{1,2*}

¹School of Artificial Intelligence, ²State Key Laboratory of EMIM, Xidian University
<https://yzc-ippl.github.io/FG-IAA/>

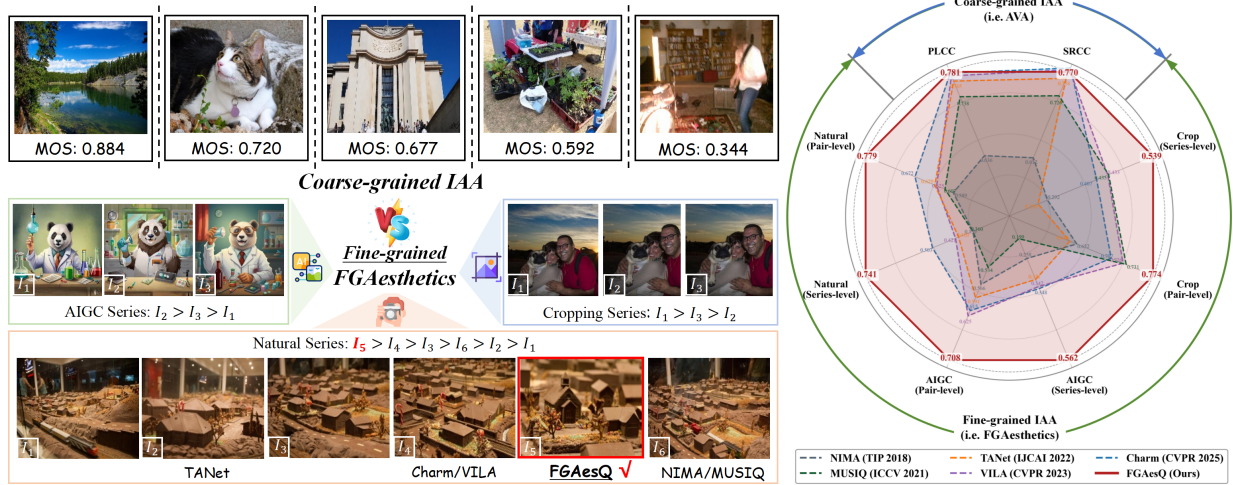


Figure 1. **Which image is aesthetically more pleasing?** We introduce FGAesthetics, a benchmark for Fine-grained Image Aesthetic Assessment that discriminates subtle aesthetic differences among similar images in photo series. It differs from previous coarse-grained datasets, e.g., AVA, where images with notable differences are evaluated independently on an absolute scale. This enables FGAesQ, a novel IAA model, to achieve accurate aesthetic assessment in fine-grained scenarios while maintaining robust coarse-grained evaluation.

Abstract

Image aesthetic assessment (IAA) has extensive applications in content creation, album management, and recommendation systems, etc. In such applications, it is commonly needed to pick out the most aesthetically pleasing image from a series of images with subtle aesthetic variations, a topic we refer to as fine-grained IAA. Unfortunately, state-of-the-art IAA models are typically designed for coarse-grained evaluation, where images with notable aesthetic differences are evaluated independently on an absolute scale. These models are inherently limited in discriminating fine-grained aesthetic differences. To address the dilemma, we contribute **FGAesthetics**, a fine-grained IAA database with 32,217 images organized into 10,028 series, which are sourced from diverse categories including Nat-

ural, AIGC, and Cropping. Annotations are collected via pairwise comparisons within each series. We also devise Series Refinement and Rank Calibration to ensure the reliability of data and labels. Based on FGAesthetics, we further propose **FGAesQ**, a novel IAA framework that learns discriminative aesthetic scores from relative ranks through Difference-preserved Tokenization (DiffToken), Comparative Text-assisted Alignment (CTAlign), and Rank-aware Regression (RankReg). FGAesQ enables accurate aesthetic assessment in fine-grained scenarios while still maintains competitive performance in coarse-grained evaluation. Extensive experiments and comparisons demonstrate the superiority of the proposed method.

1. Introduction

“The difference between something good and something great is attention to detail.” —Charles R. Swindoll

[†]Equal Contribution.

^{*}Corresponding Author.

Table 1. Comparison between the proposed FGAesthetics and representative IAA datasets.

Dataset	Year	Num. Img	Data Type	Img Source	Label Type	Evaluation Concern
CUHK-PQ [25]	2011	17,673	Single	Natural	Classification	Aesthetic Classification
AVA [26]	2012	255,530	Single	Natural	MOS	Aesthetic Scoring
AADB [21]	2016	10,000	Single	Natural	MOS	Aesthetic Attributes
TAD66K [11]	2022	66,327	Single	Natural/Art	MOS	Theme-specific Aesthetics
BAID [48]	2023	60,337	Single	Art	MOS	Artistic Aesthetics
ICAA17K [12]	2023	17,726	Single	Natural	MOS	Color Aesthetics
AesBench [16]	2024	2,800	Single	Natural/AI/Art	Description	MLLM’s Aesthetic Perception
FGAesthetics	2025	32,217	Series	Natural/AI/Crop	Rankings	Fine-grained Aesthetics

Aesthetics has emerged as a pivotal focus in the creation and consumption of visual content. In view of this, image aesthetic assessment (IAA) has witnessed notable research growth [3, 8, 16, 18], with extensive applications in image recommendation [34, 45], AI generation guidance [2, 46], album management [7, 23] and smart photography [18, 42]. In these scenarios, we often need to handle photo series that have the same semantic meaning but exhibit subtle aesthetic differences. This creates an urgent demand for accurate aesthetic evaluation capable of measuring and discriminating these nuanced differences, a challenge we define as **Fine-grained Image Aesthetic Assessment (FG-IAA)**.

In the past few years, numerous IAA datasets have been released, along with corresponding evaluation algorithms. Early benchmarks, such as CUHK-PQ [25], categorized images into high and low aesthetics. During this period, hand-crafted features were typically employed in aesthetic modeling [6, 19]. Subsequently, deep learning methods have been widely adopted to uncover common aesthetic criteria embedded within large datasets [3, 24]. AVA [26], due to its extensive scale, has become the most popular IAA benchmark. Recently, there has been deeper exploration into specific aesthetic dimensions, such as color [12] and theme [11]. The more recent prevalence of Multimodal Large Language Models (MLLMs) has also prompted researchers to explore their aesthetic perception capabilities [16, 53].

While existing benchmarks offer valuable insights, they typically evaluate images with notable aesthetic differences independently on an absolute scale, as illustrated in Tab. 1. This inherent limitation challenges the current IAA models in fine-grained scenarios. FG-IAA presents two major challenges: (1) **Semantic Interference**: strong semantic similarities in image series hinder extracting fine-grained aesthetic differences, especially that most deep models are pre-trained for semantic tasks. (2) **Subtle Variations**: minor and diverse aesthetic differences, e.g., slight color and composition changes, require models to have robust discriminative aesthetic representations. To address these challenges, we contribute **FGAesthetics**, a benchmark specifically designed for fine-grained aesthetics, comprising 32,217 im-

ages organized into 10,028 series with aesthetic ranking labels. To ensure diversity, we collect image series from three distinct sources: Natural, AIGC, and Aesthetic cropping. These series undergo rigorous filtering via a Metrics-MLLMs-Human refinement protocol, avoiding images that are either visually significantly dissimilar or indistinguishable. Human annotators then perform pairwise comparisons within each series, where pairs with ambiguous relative ordering are filtered to calibrate the global rankings and produce the final FGAesthetics dataset.

Building on FGAesthetics, we further propose **FGAesQ**, a new IAA model that enables accurate aesthetic assessment in fine-grained scenarios while maintaining robust performance in coarse-grained evaluation (Fig. 1-right). This is achieved by learning discriminative aesthetic scores from relative ranks, where coarse-grained data establishes foundational aesthetic perception and fine-grained data refines the regression space for subtle aesthetic distinctions. Specifically, we introduce Difference-preserved Tokenization (DiffToken) that maintains distinctive details between similar images while scaling homogeneous regions. Comparative Text-assisted Alignment (CTAlign) is designed to further enhance the discrimination of visual representations. Finally, we develop Rank-aware Regression (RankReg), which leverages aesthetic rankings to calibrate score predictions, ensuring consistency between absolute assessments and relative aesthetic ordering.

The contributions of this work are three-fold:

- We define Fine-grained Image Aesthetic Assessment and contribute FGAesthetics comprising 32,217 images from diverse sources including Natural, AIGC, and Cropping, organized into 10,028 series with aesthetic rankings.
- We propose FGAesQ, a novel IAA model that learns discriminative scores from relative ranks, achieving accurate aesthetic assessment in fine-grained scenarios while maintaining robust coarse-grained evaluation.
- Through extensive experiments and comparative analysis, we reveal fundamental limitations of current IAA methods in capturing fine-grained aesthetic differences and demonstrate the superiority of FGAesQ.

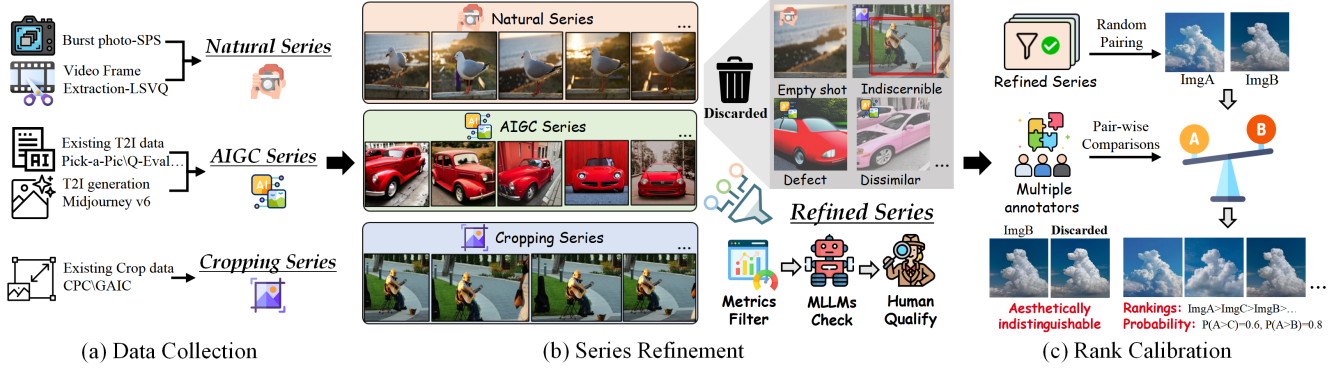


Figure 2. Overview of the construction pipeline for **FGAesthetics**. The pipeline consists of three stages: (a) Data Collection. Visually similar photo series are collected from three distinct sources: Natural, AIGC, and Cropping. (b) Series Refinement. Noisy series data undergo rigorous filtering using a Metric-MLLMs-Human refinement protocol. (c) Rank Calibration. Pairwise comparisons are annotated within each series, excluding data that cannot be aesthetically distinguished to obtain calibrated aesthetic rankings.

2. Related Work

2.1. Image Aesthetic Assessment Datasets

In the past few years, a proliferation of datasets have been developed for image aesthetic assessment, with representative benchmarks summarized in Tab. 1. Early datasets are designed for different aesthetic tasks, with CUHK-PQ [25] for binary classification and AVA [26] for score regression, where AVA remains the most widely used benchmark due to its large scale. Then, specific aesthetic dimensions have been explored: AADB [21] targets aesthetic attributes, e.g., lighting and depth of field; TAD66K [11] focuses on theme-specific aesthetics; BAID [48] addresses artistic aesthetics; and ICAA17K [12] emphasizes color aesthetics. With the emergence of Multimodal Large Language Models (MLLMs), benchmarks like AesBench [16] have been developed to evaluate their aesthetic perception capabilities.

The above benchmarks focus on the holistic aesthetic assessment of individual images, making them unsuitable for fine-grained evaluation scenarios, while related datasets have not been thoroughly studied due to open-source limitations. Chang *et al.* [5] proposed the Series Photo Selection task for burst photography scenarios, but the partially open-sourced dataset limits its development. Ren *et al.* [28] introduced the innovative Best Frame Selection task to identify the most aesthetically pleasing frames from short videos, yet the data remains inaccessible. In this study, we define the task of fine-grained image aesthetic assessment, and contribute FGAesthetics with diverse data types including Natural, AIGC, and Cropping, addressing the gap for fine-grained evaluation scenarios.

2.2. Image Aesthetic Assessment Models

Early IAA models relied on hand-crafted features and simple machine learning techniques, mainly drawing inspirations from intuitive judgments of image aesthetics and

widely accepted photography rules [6, 19]. With the advent of deep learning, IAA methods began leveraging deep neural networks to identify common aesthetic criteria in large datasets. NIMA [36] used EMD-based loss to train deep models for aesthetic distribution prediction. TANet [11] and TMCR [44] explored the intricate coupling of aesthetics and themes. VILA [18] and AesCLIP [31] achieved aesthetic evaluation by leveraging user-generated aesthetic reviews. MUSIQ [17] and Charm [3] address the fixed shape constraint of Vision Transformers (ViTs) architectures, enabling variable-sized inputs that preserve compositional integrity for more accurate aesthetics modeling. Recently, MLLM-based aesthetic scorers have been explored, with Q-Align [41] and UNIAA [53] using discrete level labels to guide MLLMs in aesthetic score regression. While these models have achieved significant progress in coarse-grained aesthetic evaluation for images with notable aesthetic differences on an absolute scale, their effectiveness on fine-grained scenarios remains largely unexplored. In this study, we address this and propose FGAesQ, a novel IAA framework with superior performance on fine-grained scenarios while still maintains robust coarse-grained evaluation.

3. FGAesthetics

In this section, we detail FGAesthetics, with the construction pipeline illustrated in Fig. 2. Throughout the benchmark, we design multiple strategies to ensure diversity and reliability. We will elaborate on the construction process from three aspects: data collection, series refinement, and rank calibration, followed by a statistical analysis.

3.1. Data Collection

To ensure diversity and comprehensive evaluation of fine-grained aesthetics, we collect images from diverse sources. For natural image series, we sample from two sources: burst

photographs capturing identical scenes from the SPS [5], and sequential frames extracted from videos in the LSVQ [49]. For AI-generated content (AIGC) series, we primarily leverage text-to-image data where images generated from same text prompts form a series. This data is mainly sampled from established T2I evaluation benchmarks, including Pick-a-pic [20], Q-Eval-100K [52], and NIGHTS [9]. We also utilize advanced proprietary generative models, such as Midjourney v6 [14], to generate series by varying parameters. Additionally, previous IAA research has demonstrated the significant impact of varying resolutions, particularly aspect ratio, on aesthetic modeling [3, 17]. To incorporate this factor in fine-grained IAA, we include cropping series derived from datasets containing dense cropping variations of the same image, such as CPC [40] and GAIC [50]. We ensured balanced sampling across all three categories, with detailed source distribution maps provided in the Appendix.

3.2. Series Refinement

To ensure that series data contains visually similar yet distinguishable images, we design a Metrics-MLLMs-Human refinement protocol to filter each collection. For Metrics Filtering, both generic and domain-specific measures are utilized to screen the data. Specifically, SSIM [39] quantifies similarity between images within each series, with samples below threshold values being removed. For cropping, IoU [29] is utilized to prevent indistinguishable cropping frames. For AIGC series, T2I alignment scores identify and eliminate obviously dissimilar images. Given the powerful contextual understanding capabilities of MLLMs [35], we also employ Gemini-2.5-pro [37] to validate the filtered series by providing all images within each series and prompting it to check data based on visual similarity and contextual coherence. Finally, all series undergo qualification by five human annotators to ensure data quality. This rigorous multi-stage process yields high-quality fine-grained series data for the subsequent aesthetic ranking annotation. Implementation details of metrics filtering, the instructions for MLLMs check using Gemini, and the operational interface for human qualify are included in the Appendix.

3.3. Rank Calibration

Based on the refined data, we perform pairwise comparisons within each series to obtain global aesthetic rankings. Specifically, for a series of length n , a total of C_n^2 image pairs are generated. Each pair is evaluated by 10 trained annotators for aesthetic comparison, determining which image is superior or indistinguishable. This annotation methodology offers three key advantages: (1) Pairwise aesthetic comparisons yield more reliable annotations compared to absolute scoring or full series ranking. (2) It facilitates the identification and removal of aesthetically indistinguishable samples. (3) The probability of pairwise comparisons be-

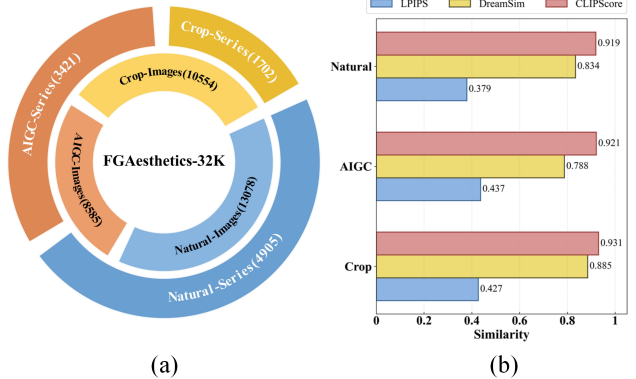


Figure 3. Statistical analysis of FGAesthetics. (a) Image and series count distribution across Natural, AIGC, and Cropping. (b) Within-series similarity distributions measured by LPIPS (low-level) [51], DreamSim (mid-level) [9], and CLIPScore (high-level) [13] across three sources. Note that LPIPS and DreamSim are subtracted from 1, ensuring consistent polarity with CLIPScore, where higher values indicate greater similarity.

comes directly measurable, e.g., 0.5 indicates no consensus (half preferring each image) and warrants filtering while 0.9 suggests clear aesthetic superiority. Based on the collected pairwise annotations, we derive the global ranking labels, while filtering out indistinguishable samples and series with comparison conflicts. Note that for sampled data from SPS [5], originally annotated through pairwise comparisons, fine-grained rankings can be directly derived without additional human annotation.

3.4. Statistics of FGAesthetics

During data collection, we gather 106,632 images, which are filtered to 32,588 through rigorous series refinement. Following rank calibration, the final dataset comprises 32,217 images organized into 10,028 series with lengths ranging from 2 to 10, forming FGAesthetics. Fig. 3-(a) presents image and series count distribution across Natural, AIGC, and Cropping. The analysis shows relatively balanced image distribution, with Cropping containing more long series, as multiple crops from the same source image naturally form longer sequences with finer aesthetic distinctions. To quantitatively verify the fine-grained nature of our dataset, we measure within-series similarity using LPIPS (low-level) [51], DreamSim (mid-level) [9], and CLIPScore (high-level) [13], as summarized in Fig. 3-(b). Results reveal consistent trends across three sources: high semantic similarity (CLIPScore > 0.91), contrasted with moderate patch-level similarity (LPIPS between 0.379 and 0.437). This confirms that images within series maintain semantic coherence while exhibiting fine-grained visual differences that influence aesthetic perception.

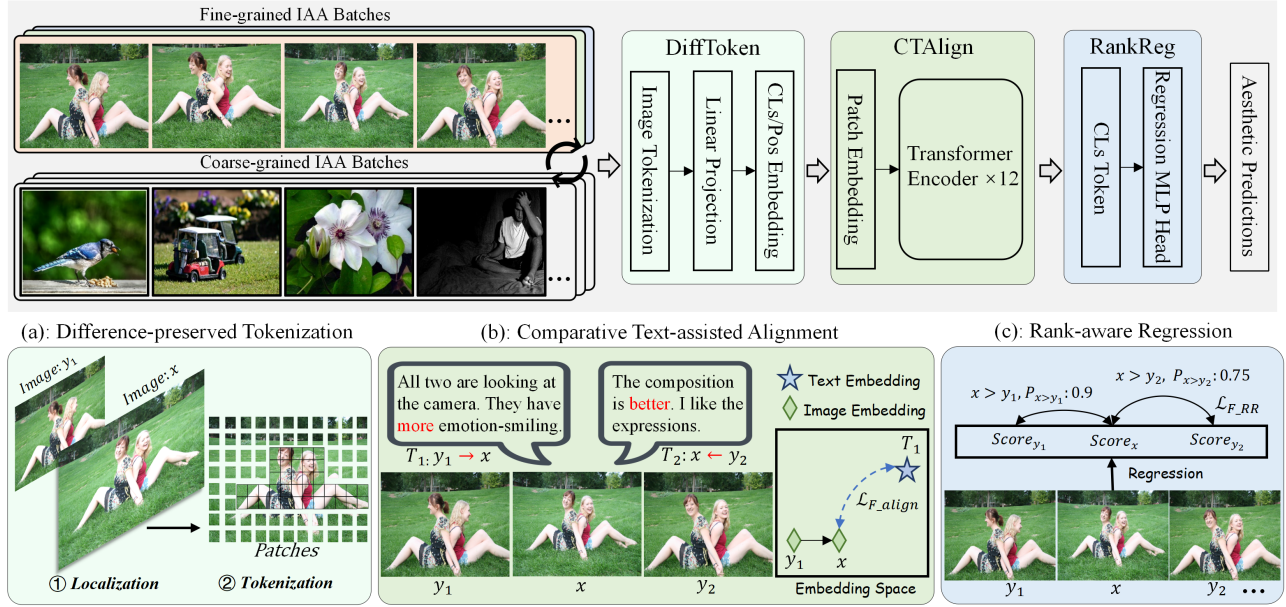


Figure 4. Overall pipeline of the proposed **FGAesQ**. FGAesQ learns discriminative aesthetic scores from relative ranks through three modules: (a) Difference-preserved Tokenization (DiffToken) selectively maintains difference regions at their original resolution while downscaling others. (b) Comparative Text-assisted Alignment (CTAlign) achieves distinctive aesthetic visual representations. (c) Rank-aware Regression (RankReg) rectifies the coarse-grained score regression with fine-grained aesthetic rankings.

4. FGAesQ

Building upon FGAesthetics, we propose FGAesQ, a novel IAA framework that enables accurate aesthetic assessment in fine-grained scenarios while maintaining robust coarse-grained evaluation. The overall pipeline is shown in Fig. 4.

Overall architecture. Fine-grained aesthetic discrimination is fundamentally grounded on coarse-grained aesthetic perception. Therefore, we propose to leverage fine-grained ranks to enhance scoring discriminability, enabling unified capabilities for both coarse- and fine-grained aesthetic evaluations. Specifically, we train a Vision Transformer [27] using both coarse- and fine-grained aesthetic data: the coarse batch contains distinct images with absolute scores from existing IAA datasets, while the fine batch contains visually similar image series with ranking labels. To address the Semantic Interference and Subtle Variations challenges in FG-IAA, we introduce difference-preserved tokenization (DiffToken), comparative text-assisted alignment (CTAlign) and rank-aware regression (RankReg), based on which discriminative aesthetic representations can be learned.

4.1. Difference-preserved Tokenization

For fine-grained input, images within a series share substantial semantic similarity, with only limited regions exhibiting difference significantly influencing their aesthetic ranking. This characteristic is empirically supported by the low perceptual similarity measured by LPIPS (operat-

ing on 64×64 patches) shown in Fig. 3-(b). Recognizing that these aesthetics-decisive regions contain critical cues, we design Difference-preserved Tokenization (DiffToken), which maintains their details while downscaling others. This approach enables the visual model to focus computational resources on perceptually significant areas that drive fine-grained aesthetic discrimination.

DiffToken first localizes aesthetics-decisive regions and then performs mix-resolution tokenization. Specifically, for a fine-grained batch containing k series: $B_F \{s_1, \dots, s_k\}$, we randomly sample an image pair (x, y_1) from a series, where x is the target image to be tokenized and y_1 is the reference image. Using the longer edge of x as the baseline, y_1 is aligned through scaling while maintaining its original aspect ratio. Both images are then partitioned into patches at a multiple (e.g., $2\times$) of the standard ViT patch size. Based on this partition, the similarity between corresponding patches is computed using RGB-channel SSIM [39]:

$$s_{i,j} = \text{SSIM}(P_{i,j}^x, P_{i,j}^{y_1}), \quad (1)$$

where $P_{i,j}^x, P_{i,j}^{y_1}$ denote patches at position (i, j) in images x and y_1 respectively. We then sort all patches by similarity scores $s_{i,j}$ and identify the aesthetics-decisive regions by selecting patches with similarity below a threshold τ :

$$D = \{(i, j) \mid s_{i,j} < \tau, \tau = \text{percentile}(s, p)\}, \quad (2)$$

where p is the percentile parameter controlling the proportion of patches identified as aesthetics-decisive regions.

Based on identified aesthetics-decisive regions, we implement difference-preserved tokenization. Patches within set D are partitioned at the original ViT patch resolution to preserve details. Remaining patches are scaled to required size with random dropping applied to satisfy token count constraints. Additionally, we accommodate varying input aspect ratios through bilinear interpolation of position embeddings during the tokenization process [3, 10, 17, 30, 38]. This ensures both high-fidelity local difference and comprehensive global composition.

4.2. Comparative Text-assisted Alignment

Based on difference-preserved tokens, we further utilize comparative textual descriptions to orient the visual model toward fine-grained aesthetic differences, thereby enhancing discrimination capabilities. To obtain these descriptions while minimizing human annotation burden, we leverage the robust reasoning capabilities of MLLMs. Specifically, image pairs with human-annotated aesthetic ranking labels are utilized to instruct GPT-4o [1], eliciting comparative reasoning with explicitly contrastive vocabulary. For Cropping and AIGC series, original images and text prompts also serve as context to ensure high-quality textual outputs. The detailed prompt engineering for reasoning generation is provided in the Appendix.

Given $T_1 : x \leftarrow y_1$ representing the comparative text of target image x relative to reference y_1 , we extract its embedding using text encoder of CLIP [27] and align it with the visual embedding difference between the two images. This alignment is achieved by minimizing the following loss:

$$\mathcal{L}_{F_align} = \cos(E_v(x) - E_v(y_1), E_t(T_1)), \quad (3)$$

where E_v , E_t denote the vision and text encoders respectively, and $\cos()$ is the cosine similarity. Note that texts are only utilized during the training process, and only the learned image encoder is used during inference.

4.3. Rank-aware Regression

With the aligned visual representations, human-annotated aesthetic ranking labels within each series are utilized to refine score regression. Specifically, for an image pair (x, y_1) from a series, absolute scores $(Score_x, Score_{y_1})$ are first obtained through a regression head. We then employ the Bradley-Terry model [4] to compute the probability that target image x is aesthetically superior to reference y_1 :

$$P_{(x \succ y_1)} = \frac{e^{Score_x}}{e^{Score_x} + e^{Score_{y_1}}}. \quad (4)$$

The above operation is performed for all pairs within the series to obtain the complete predicted probability distribution $\mathbf{P}' = \{P_{(x \succ y_1)}, P_{(x \succ y_2)}, \dots\}$. The ListMLE [43] is used as

loss function to align it with the ground truths \mathbf{P} :

$$\mathcal{L}_{F_RR}(\mathbf{P}', \mathbf{P}) = - \sum_{j=1}^n \log \frac{e^{\mathbf{P}'(r_i)}}{\sum_{j=i}^n e^{\mathbf{P}'(r_j)}}, \quad (5)$$

where r represents the ranking order derived from \mathbf{P} , $\mathbf{P}'(r_i)$ is the predicted probability at position i in this ranking, and n is the cardinality of \mathbf{P}' . The loss \mathcal{L}_{F_RR} simultaneously optimizes both the ranking accuracy of series elements and the calibration of probability estimates between pairs.

4.4. Training of FGAesQ

FGAesQ adopts a two-stage training strategy: pre-training on coarse-grained data followed by joint learning across both granularities. The model is first pre-trained using coarse-grained IAA data to establish foundational aesthetic perception capability. Similar to previous IAA methods [3, 11, 18, 32, 33, 36, 44, 47], the Earth Mover’s Distance (EMD) loss is employed to guide the model in predicting aesthetic scores for single images, denoted as \mathcal{L}_{C_EMD} . Building upon this, we perform a joint learning that alternately optimizes the model using coarse- and fine-grained IAA batches, enabling fine-grained ranking to refine coarse-grained scoring. This alternating training process can be formatted as:

$$\mathcal{L} = \underbrace{\delta \cdot (\lambda \mathcal{L}_{F_align} + \mathcal{L}_{F_RR})}_{\text{Fine-grained}} + \underbrace{(1 - \delta) \cdot \mathcal{L}_{C_EMD}}_{\text{Coarse-grained}}, \quad (6)$$

where δ represents a binary alternating indicator, and λ is a balancing coefficient. The optimization of FGAesQ proceeds through momentum-based updates, ensuring smooth optimization across different learning objectives.

5. Experiments

5.1. Experimental Settings

Implementation Details. For FGAesQ, we utilize visual encoder (ViT-B/16) of CLIP [27] as the backbone, where AVA [26] provides coarse-grained data and FGAesthetics enables fine-grained training. For coarse-grained pre-training, we use a learning rate of $2e-5$, batch size of 128, and train for 3 epochs. For joint learning, we maintain a learning rate of $2e-5$ with weight decay of $5e-5$, using batch sizes of approximately 64 for fine-grained data (with minor variations due to series length) and 128 for coarse-grained, with λ set to 10. The momentum update coefficients are set to 0.615 and 0.8 respectively, with training continuing for 7 epochs on an A800 GPU. For the DiffToken module, we employ 32×32 patches for difference localization with p set to 0.5, further details on these settings are in the Appendix.

Evaluation Setting. We employ an 8:1:1 train-validation-test split for FGAesthetics, ensuring balanced distribution of all three image sources. For fine-grained evaluation, we

Table 2. Performance comparison between the proposed FGAesQ and state-of-the-art IAA methods on FGAesthetics. Results are reported across all three image sources (Natural, AIGC, and Cropping) for both pair-level and series-level evaluations. Model parameter counts are also provided. The top two results are highlighted in **bold** and underlined, respectively.

Methods	Params	Natural				AIGC				Cropping			
		Pair-level		Series-level		Pair-level		Series-level		Pair-level		Series-level	
		Acc	FI	s-Acc	s-SRCC	Acc	FI	s-Acc	s-SRCC	Acc	FI	s-Acc	s-SRCC
NIMA (TIP 2018) [36]	54.3M	0.589	0.588	0.493	0.225	0.566	0.565	0.379	0.137	0.655	0.649	0.272	0.312
MLSP (CVPR 2019) [15]	114 M	0.608	0.607	0.531	0.255	0.604	0.602	0.414	0.182	0.710	0.710	0.396	0.430
MUSIQ (ICCV 2021) [17]	78.6M	0.607	0.606	0.487	0.233	0.535	0.532	0.344	0.054	0.731	0.731	0.375	0.495
TANet (IJCAI 2022) [11]	13.9M	0.629	0.628	0.539	0.281	0.591	0.590	0.447	0.195	0.641	0.641	0.244	0.295
VILA (CVPR 2023) [18]	303M	0.625	0.625	0.546	0.296	0.625	0.624	0.438	0.245	0.726	0.726	0.423	0.443
Charm (CVPR 2025) [3]	85.7M	0.672	0.672	0.602	0.404	0.616	0.614	0.448	0.247	0.707	0.707	0.381	0.432
Q-Align (ICML 2024) [41]	8.20B	0.711	0.711	0.676	0.496	0.646	0.646	0.462	0.310	0.738	0.739	0.413	0.487
UNIAA (arXiv 2024) [53]	7.06B	0.709	0.708	0.656	0.486	0.640	0.639	0.486	0.256	0.675	0.670	0.300	0.386
RealQA (arXiv 2025) [22]	8.29B	0.658	0.666	0.593	0.382	0.656	0.656	0.464	0.308	0.605	0.613	0.275	0.235
NIMA (Fine-tuned) [36]	54.3M	0.643	0.644	0.536	0.312	0.598	0.597	0.429	0.196	0.708	0.704	0.277	0.352
MUSIQ (Fine-tuned) [17]	78.6M	0.654	0.654	0.545	0.356	0.572	0.568	0.386	0.145	<u>0.770</u>	<u>0.770</u>	<u>0.487</u>	<u>0.556</u>
VILA (Fine-tuned) [18]	303M	0.693	0.692	0.643	0.430	0.650	0.647	0.504	0.291	0.714	0.710	0.373	0.439
Charm (Fine-tuned) [3]	85.7M	0.723	0.723	0.670	0.474	0.620	0.619	0.478	0.254	0.755	0.755	0.467	0.517
FGAesQ (w/o DiffToken)	86.3M	<u>0.773</u>	<u>0.773</u>	<u>0.720</u>	<u>0.664</u>	0.688	0.686	<u>0.517</u>	<u>0.442</u>	0.764	0.763	0.483	0.537
FGAesQ (w DiffToken)	86.3M	0.779	0.779	0.753	0.729	0.709	0.707	0.561	0.482	0.774	0.773	0.488	0.590

conduct pair-level and series-level testings. At pair-level, we use *Acc* and *FI* as metrics to assess local discrimination within series. For series-level, we measure the accuracy of identifying the most aesthetic image and use SRCC for ranking correlation. Considering longer series pose greater challenges, we employ length-weighted metrics, denoted as *s-Acc* and *s-SRCC*. For coarse-grained evaluation, we adopt the standard SRCC and PLCC. Competing methods contain CNN-based, ViT-based, and MLLM-based IAA models.

5.2. Performance Evaluation

Benchmark Results on FGAesthetics. Tab. 2 lists the comparative results of FGAesQ against existing IAA methods on FGAesthetics, from which we have several key observations. First, existing IAA models demonstrate significant performance degradation on fine-grained evaluation scenarios, particularly for series-level testing. Second, MLLM-based IAA approaches outperform traditional deep learning-based methods, with Q-Align [41] showing very encouraging results even against fine-tuned models. This stems from the enhanced fine-grained perception capabilities afforded by larger parameters. Third, input scale-focused methods [15, 17] exhibit superior performance on cropping data, with fine-tuned MUSIQ [17] achieving second-best results. Finally, FGAesQ achieves the best performance across all evaluation protocols, demonstrating superior aesthetic discrimination capabilities in FG-IAA. Additionally, we evaluate FGAesQ excluding DiffToken during inference, which operates without reference image comparison yet still maintains competitive performance.

Table 3. Balance between coarse-grained (AVA) and fine-grained (FGAesthetics) evaluations. Metrics shown are $(Acc, FI)/2$ for Pair and $(s-Acc, s-SRCC)/2$ for Series. Best in bold.

Methods	AVA		FGAesthetics	
	SRCC	PLCC	Pair	Series
NIMA (TIP 2018) [36]	0.633	0.647	0.602	0.303
MUSIQ (ICCV 2021) [17]	0.726	0.738	0.624	0.331
VILA (CVPR 2023) [18]	0.774	0.774	0.659	0.399
Charm (CVPR 2025) [3]	0.777	0.779	0.665	0.419
NIMA (Fine-tuned) [36]	0.330	0.313	0.649	0.350
	(-0.303)	(-0.334)	(+0.047)	(+0.047)
MUSIQ (Fine-tuned) [17]	0.437	0.461	0.665	0.413
	(-0.289)	(-0.277)	(+0.041)	(+0.082)
VILA (Fine-tuned) [18]	0.522	0.507	0.687	0.447
	(-0.252)	(-0.267)	(+0.028)	(+0.048)
Charm (Fine-tuned) [3]	0.470	0.472	0.699	0.477
	(-0.307)	(-0.307)	(+0.034)	(+0.058)
FGAesQ	0.770	0.781	0.753	0.600

Balance between Coarse- and Fine-grained IAA. A robust IAA model is expected to handle both coarse- and fine-grained evaluation scenarios. Tab. 3 compares performance on both tasks, where FGAesQ achieves the highest average results. Existing SOTA models fine-tuned with ranking loss show enhanced fine-grained capabilities but suffer severe coarse-grained degradation (SRCC and PLCC drops highlighted in red). In contrast, FGAesQ maintains competitive performance across both tasks, demonstrating our approach effectively learns discriminative scores from relative ranks.

Table 4. Cross-dataset validation on three IAA benchmarks: ICAA17K [12], AADB [21], and TAD66K [11]. Results for UNIAA [53] on AADB are omitted as data is used in training.

Methods	ICAA17K		AADB		TAD66K	
	SRCC	PLCC	SRCC	PLCC	SRCC	PLCC
NIMA [36]	0.629	0.629	0.365	0.371	0.392	0.370
MUSIQ [17]	0.581	0.578	0.331	0.343	0.314	0.332
VILA [18]	0.652	0.663	0.548	0.561	0.413	0.443
UNIAA [53]	0.472	0.390	-	-	0.261	0.260
Charm [3]	0.651	0.661	0.510	0.528	0.411	0.441
FGAesQ	0.653	0.674	0.562	0.571	0.423	0.455

Table 5. Ablation study on training strategies and model components. ‘w/o’ is removal of the specified training or component. Metrics are $(Acc, FI)/2$ for Pair and $(s-Acc, s-SRCC)/2$ for Series.

Methods	Coarse-grained		Fine-grained	
	SRCC	PLCC	Pair	Series
w/o Fine	0.713	0.726	0.578	0.364
w/o Coarse	0.031	0.050	0.565	0.299
Coarse Fine	0.200	0.214	0.637	0.380
w/o DiffToken	0.751	0.760	0.666	0.423
w/o CTAlign	0.770	0.780	0.747	0.581
w/o RankReg	0.769	0.781	0.742	0.571
FGAesQ	0.770	0.781	0.753	0.600

Cross-dataset Evaluation. We further conduct generalization evaluations on three IAA benchmarks, including ICAA17K [12] (color aesthetics), AADB [21] (aesthetic attributes), and TAD66K [11] (theme-specific aesthetics), as summarized in Tab. 4. FGAesQ demonstrates superior generalization across all datasets, particularly exhibiting significant advantages on AADB. This suggests that training with fine-grained aesthetic comparisons enhances the perception of aesthetic attributes, enabling more accurate evaluation.

5.3. Ablation Study

We conduct extensive ablations to validate training strategy and model components of FGAesQ, as listed in Tab. 5.

Training Strategy. We first evaluate FGAesQ with isolated training (w/o Fine and w/o Coarse). Performance drops when the corresponding training is absent, confirming the distinct nature of fine- and coarse-grained aesthetic data. The sequential training (Coarse | Fine) also shows substantial degradation, demonstrating the effectiveness of two-stage training strategy for FGAesQ.

Model Components. We further evaluate component contributions through model variants (w/o DiffToken, w/o CTAlign and w/o RankReg). Decreases in both pair-level and series-level performance demonstrate their effectiveness for fine-grained aesthetic modeling. The performance

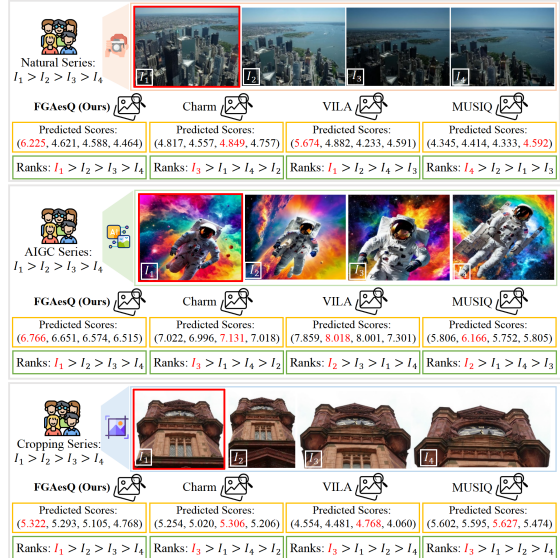


Figure 5. Visualization of evaluation results on three test series. Images arranged left-to-right in decreasing aesthetic quality. Red boxes and text indicate the best aesthetics.

drops when removing text particularly validate the value of MLLM-generated comparative descriptions. Note that w/o RankReg refers to direct ranking training.

5.4. Visual Analysis

In Fig. 5, we show the visualization results of FGAesQ, Charm [3], VILA [18], and MUSIQ [17] on three test series. FGAesQ not only accurately identifies the most aesthetic image (highlighted by red boxes), but also predicts rankings with better consistency with human annotations across the entire series. This demonstrates its superior capability in capturing fine-grained aesthetic nuances.

6. Conclusion

In this paper, we have introduced the task of fine-grained image aesthetic assessment that discriminates subtle aesthetic differences among visually similar photo series. We contribute FGAesthetics, a large-scale dataset containing diverse image series with aesthetic rankings. Experiments on FGAesthetics reveal that existing IAA methods, while achieving excellent coarse-grained evaluation, fundamentally struggle with subtle aesthetic discrimination in fine-grained scenarios. Given this limitation, we further propose FGAesQ that learns discriminative scores from relative ranks, enabling superior evaluation performance in both fine- and coarse-grained scenarios. While encouraging results have been achieved in this work, fine-grained IAA remains challenging. We hope our contributions can inspire the community to rethink the problem with more technical approaches and broader perspectives.

7. Acknowledgments

This work is supported by National Natural Science Foundation of China under Grants 62471349, 62171340, 62301378, and 625B2142, Fundamental Research Funds for the Central Universities under Grant QTZX25076 and YJSJ25004, the China Postdoctoral Science Foundation under Grant 2024M762553. We also sincerely thank all annotators for their dedicated efforts and significant contributions to the construction of the database.

References

- [1] Josh Achiam, Steven Adler, Sandhini Agarwal, Lama Ahmad, Ilge Akkaya, Florencia Leoni Aleman, Diogo Almeida, Janko Altenschmidt, Sam Altman, Shyamal Anadkat, et al. Gpt-4 technical report. *arXiv preprint arXiv:2303.08774*, 2023. 6
- [2] Ying Ba, Tianyu Zhang, Yalong Bai, Wenyi Mo, Tao Liang, Bing Su, and Ji-Rong Wen. Enhancing reward models for high-quality image generation: Beyond text-image alignment. In *Proceedings of the IEEE/CVF International Conference on Computer Vision*, pages 19022–19031, 2025. 2
- [3] Fatemeh Behrad, Tinne Tuytelaars, and Johan Wagemans. Charm: The missing piece in vit fine-tuning for image aesthetic assessment. In *Proceedings of the Computer Vision and Pattern Recognition Conference*, pages 7815–7824, 2025. 2, 3, 4, 6, 7, 8
- [4] Ralph Allan Bradley and Milton E Terry. Rank analysis of incomplete block designs: I. the method of paired comparisons. *Biometrika*, 39(3/4):324–345, 1952. 6
- [5] Huiwen Chang, Fisher Yu, Jue Wang, Douglas Ashley, and Adam Finkelstein. Automatic triage for a photo series. *ACM Transactions on Graphics (TOG)*, 35(4):1–10, 2016. 3, 4, 1
- [6] Ritendra Datta, Dhiraj Joshi, Jia Li, and James Z Wang. Studying aesthetics in photographic images using a computational approach. In *European conference on computer vision*, pages 288–301. Springer, 2006. 2, 3
- [7] Ritendra Datta, Jia Li, and James Z Wang. Algorithmic inferring of aesthetics and emotion in natural images: An exposition. In *2008 15th IEEE international conference on image processing*, pages 105–108. IEEE, 2008. 2
- [8] Yubin Deng, Chen Change Loy, and Xiaoou Tang. Image aesthetic assessment: An experimental survey. *IEEE Signal Processing Magazine*, 34(4):80–106, 2017. 2
- [9] Stephanie Fu, Netanel Y Tamir, Shobhita Sundaram, Lucy Chai, Richard Zhang, Tali Dekel, and Phillip Isola. Dreamsim: learning new dimensions of human visual similarity using synthetic data. In *Proceedings of the 37th International Conference on Neural Information Processing Systems*, pages 50742–50768, 2023. 4, 1
- [10] Jakob Drachmann Havtorn, Amélie Royer, Tijmen Blankevoort, and Babak Ehteshami Bejnordi. Msvit: Dynamic mixed-scale tokenization for vision transformers. In *Proceedings of the IEEE/CVF International Conference on Computer Vision*, pages 838–848, 2023. 6
- [11] Shuai He, Yongchang Zhang, Rui Xie, Dongxiang Jiang, and Anlong Ming. Rethinking image aesthetics assessment: Models, datasets and benchmarks. In *IJCAI*, pages 942–948, 2022. 2, 3, 6, 7, 8
- [12] Shuai He, Anlong Ming, Yaqi Li, Jinyuan Sun, ShunTian Zheng, and Huadong Ma. Thinking image color aesthetics assessment: Models, datasets and benchmarks. In *Proceedings of the IEEE/CVF International Conference on Computer Vision*, pages 21838–21847, 2023. 2, 3, 8
- [13] Jack Hessel, Ari Holtzman, Maxwell Forbes, Ronan Le Bras, and Yejin Choi. Clipscore: A reference-free evaluation metric for image captioning. In *Proceedings of the 2021 Conference on Empirical Methods in Natural Language Processing*, pages 7514–7528, 2021. 4
- [14] David Holz. Midjourney. <https://www.midjourney>, 2023. 4, 1
- [15] Vlad Hosu, Bastian Goldlücke, and Dietmar Saupe. Effective aesthetics prediction with multi-level spatially pooled features. In *proceedings of the IEEE/CVF conference on computer vision and pattern recognition*, pages 9375–9383, 2019. 7
- [16] Yipo Huang, Quan Yuan, Xiangfei Sheng, Zhichao Yang, Haoning Wu, Pengfei Chen, Yuzhe Yang, Leida Li, and Weisi Lin. Aesbench: An expert benchmark for multimodal large language models on image aesthetics perception. *arXiv preprint arXiv:2401.08276*, 2024. 2, 3
- [17] Junjie Ke, Qifei Wang, Yilin Wang, Peyman Milanfar, and Feng Yang. Musiq: Multi-scale image quality transformer. In *Proceedings of the IEEE/CVF international conference on computer vision*, pages 5148–5157, 2021. 3, 4, 6, 7, 8
- [18] Junjie Ke, Keren Ye, Jiahui Yu, Yonghui Wu, Peyman Milanfar, and Feng Yang. Vila: Learning image aesthetics from user comments with vision-language pretraining. In *Proceedings of the IEEE/CVF Conference on Computer Vision and Pattern Recognition*, pages 10041–10051, 2023. 2, 3, 6, 7, 8
- [19] Yan Ke, Xiaoou Tang, and Feng Jing. The design of high-level features for photo quality assessment. In *2006 IEEE Computer Society Conference on Computer Vision and Pattern Recognition (CVPR'06)*, pages 419–426. IEEE, 2006. 2, 3
- [20] Yuval Kirstain, Adam Polyak, Uriel Singer, Shahbuland Matiana, Joe Penna, and Omer Levy. Pick-a-pic: An open dataset of user preferences for text-to-image generation. *Advances in neural information processing systems*, 36:36652–36663, 2023. 4, 1
- [21] Shu Kong, Xiaohui Shen, Zhe Lin, Radomir Mech, and Charless Fowlkes. Photo aesthetics ranking network with attributes and content adaptation. In *European conference on computer vision*, pages 662–679. Springer, 2016. 2, 3, 8
- [22] Mingxing Li, Rui Wang, Lei Sun, Yancheng Bai, and Xi-angxiang Chu. Next token is enough: Realistic image quality and aesthetic scoring with multimodal large language model. *arXiv preprint arXiv:2503.06141*, 2025. 7
- [23] Alexander C Loui and Andreas Savakis. Automated event clustering and quality screening of consumer pictures for digital albuming. *IEEE Transactions on Multimedia*, 5(3): 390–402, 2003. 2

- [24] Xin Lu, Zhe Lin, Xiaohui Shen, Radomir Mech, and James Z Wang. Deep multi-patch aggregation network for image style, aesthetics, and quality estimation. In *Proceedings of the IEEE international conference on computer vision*, pages 990–998, 2015. 2
- [25] Wei Luo, Xiaogang Wang, and Xiaoou Tang. Content-based photo quality assessment. In *2011 international conference on computer vision*, pages 2206–2213. IEEE, 2011. 2, 3
- [26] Naila Murray, Luca Marchesotti, and Florent Perronnin. Ava: A large-scale database for aesthetic visual analysis. In *2012 IEEE conference on computer vision and pattern recognition*, pages 2408–2415. IEEE, 2012. 2, 3, 6, 4
- [27] Alec Radford, Jong Wook Kim, Chris Hallacy, Aditya Ramesh, Gabriel Goh, Sandhini Agarwal, Girish Sastry, Amanda Askell, Pamela Mishkin, Jack Clark, et al. Learning transferable visual models from natural language supervision. In *International conference on machine learning*, pages 8748–8763. PmLR, 2021. 5, 6
- [28] Jian Ren, Xiaohui Shen, Zhe Lin, and Radomir Mech. Best frame selection in a short video. In *Proceedings of the IEEE/CVF Winter Conference on applications of computer vision*, pages 3212–3221, 2020. 3
- [29] Hamid Rezaatofighi, Nathan Tsoi, JunYoung Gwak, Amir Sadeghian, Ian Reid, and Silvio Savarese. Generalized intersection over union: A metric and a loss for bounding box regression. In *Proceedings of the IEEE/CVF conference on computer vision and pattern recognition*, pages 658–666, 2019. 4
- [30] Tomer Ronen, Omer Levy, and Avram Golbert. Vision transformers with mixed-resolution tokenization. In *Proceedings of the IEEE/CVF Conference on Computer Vision and Pattern Recognition*, pages 4613–4622, 2023. 6
- [31] Xiangfei Sheng, Leida Li, Pengfei Chen, Jinjian Wu, Weisheng Dong, Yuzhe Yang, Liwu Xu, Yaqian Li, and Guangming Shi. Aesclip: Multi-attribute contrastive learning for image aesthetics assessment. In *Proceedings of the 31st ACM International Conference on Multimedia*, pages 1117–1126, 2023. 3
- [32] Xiangfei Sheng, Zhichao Duan, Xiaofeng Pan, Yipo Huang, Zhichao Yang, Pengfei Chen, and Leida Li. Tuningiqqa: Fine-grained blind image quality assessment for livestreaming camera tuning. *arXiv preprint arXiv:2508.17965*, 2025. 6
- [33] Xiangfei Sheng, Xiaofeng Pan, Zhichao Yang, Pengfei Chen, and Leida Li. Fine-grained image quality assessment for perceptual image restoration. *arXiv preprint arXiv:2508.14475*, 2025. 6
- [34] Wei-Tse Sun, Ting-Hsuan Chao, Yin-Hsi Kuo, and Winston H Hsu. Photo filter recommendation by category-aware aesthetic learning. *IEEE Transactions on Multimedia*, 19(8): 1870–1880, 2017. 2
- [35] Yan Tai, Weichen Fan, Zhao Zhang, and Ziwei Liu. Link-context learning for multimodal llms. In *Proceedings of the IEEE/CVF Conference on Computer Vision and Pattern Recognition*, pages 27176–27185, 2024. 4
- [36] Hossein Talebi and Peyman Milanfar. Nima: Neural image assessment. *IEEE transactions on image processing*, 27(8): 3998–4011, 2018. 3, 6, 7, 8
- [37] Gemini Team, Rohan Anil, Sebastian Borgeaud, Jean-Baptiste Alayrac, Jiahui Yu, Radu Soricut, Johan Schalkwyk, Andrew M Dai, Anja Hauth, Katie Millican, et al. Gemini: a family of highly capable multimodal models. *arXiv preprint arXiv:2312.11805*, 2023. 4, 1
- [38] Jianyi Wang, Kelvin CK Chan, and Chen Change Loy. Exploring clip for assessing the look and feel of images. In *Proceedings of the AAAI conference on artificial intelligence*, pages 2555–2563, 2023. 6
- [39] Zhou Wang, Alan C Bovik, Hamid R Sheikh, and Eero P Simoncelli. Image quality assessment: from error visibility to structural similarity. *IEEE transactions on image processing*, 13(4):600–612, 2004. 4, 5
- [40] Zijun Wei, Jianming Zhang, Xiaohui Shen, Zhe Lin, Radomir Mech, Minh Hoai, and Dimitris Samaras. Good view hunting: Learning photo composition from dense view pairs. In *Proceedings of the IEEE conference on computer vision and pattern recognition*, pages 5437–5446, 2018. 4, 1
- [41] Haoning Wu, Zicheng Zhang, Weixia Zhang, Chaofeng Chen, Liang Liao, Chunyi Li, Yixuan Gao, Annan Wang, Erli Zhang, Wenxiu Sun, et al. Q-align: Teaching llms for visual scoring via discrete text-defined levels. In *International Conference on Machine Learning*, pages 54015–54029. PMLR, 2024. 3, 7
- [42] Jiarui Wu, Yujin Wang, Lingen Li, Fan Zhang, and Tianfan Xue. Goal conditioned reinforcement learning for photo finishing tuning. *Advances in Neural Information Processing Systems*, 37:46294–46318, 2024. 2
- [43] Fen Xia, Tie-Yan Liu, Jue Wang, Wensheng Zhang, and Hang Li. Listwise approach to learning to rank: theory and algorithm. In *Proceedings of the 25th international conference on Machine learning*, pages 1192–1199, 2008. 6
- [44] Zhichao Yang, Leida Li, Pengfei Chen, Jinjian Wu, and Weisheng Dong. Semantics-aware image aesthetics assessment using tag matching and contrastive ranking. In *Proceedings of the 32nd ACM International Conference on Multimedia*, pages 2632–2641, 2024. 3, 6
- [45] Zhichao Yang, Leida Li, Yuzhe Yang, Yaqian Li, and Weisi Lin. Multi-level transitional contrast learning for personalized image aesthetics assessment. *IEEE Transactions on Multimedia*, 26:1944–1956, 2024. 2
- [46] Zhichao Yang, Tianjiao Gu, Jianjie Wang, Feiyu Lin, Xiangfei Sheng, Pengfei Chen, and Leida Li. Longt2ibench: A benchmark for evaluating long text-to-image generation with graph-structured annotations. *arXiv preprint arXiv:2512.09271*, 2025. 2
- [47] Zhichao Yang, Leida Li, Pengfei Chen, Jinjian Wu, and Giuseppe Valenzise. Language-guided visual perception disentanglement for image quality assessment and conditional image generation. *arXiv preprint arXiv:2503.02206*, 2025. 6
- [48] Ran Yi, Haoyuan Tian, Zhihao Gu, Yu-Kun Lai, and Paul L Rosin. Towards artistic image aesthetics assessment: a large-scale dataset and a new method. In *Proceedings of the IEEE/CVF Conference on Computer Vision and Pattern Recognition*, pages 22388–22397, 2023. 2, 3
- [49] Zhenqiang Ying, Maniratnam Mandal, Deepti Ghadiyaram, and Alan Bovik. Patch-vq: patching up the video qual-

- ity problem. In *Proceedings of the IEEE/CVF conference on computer vision and pattern recognition*, pages 14019–14029, 2021. [4](#), [1](#)
- [50] Hui Zeng, Lida Li, Zisheng Cao, and Lei Zhang. Reliable and efficient image cropping: A grid anchor based approach. In *Proceedings of the IEEE/CVF conference on computer vision and pattern recognition*, pages 5949–5957, 2019. [4](#), [1](#)
- [51] Richard Zhang, Phillip Isola, Alexei A Efros, Eli Shechtman, and Oliver Wang. The unreasonable effectiveness of deep features as a perceptual metric. In *Proceedings of the IEEE conference on computer vision and pattern recognition*, pages 586–595, 2018. [4](#)
- [52] Zicheng Zhang, Tengchuan Kou, Shushi Wang, Chunyi Li, Wei Sun, Wei Wang, Xiaoyu Li, Zongyu Wang, Xuezhi Cao, Xiongkuo Min, et al. Q-eval-100k: Evaluating visual quality and alignment level for text-to-vision content. In *Proceedings of the Computer Vision and Pattern Recognition Conference*, pages 10621–10631, 2025. [4](#), [1](#)
- [53] Zhaokun Zhou, Qiulin Wang, Bin Lin, Yiwei Su, Rui Chen, Xin Tao, Amin Zheng, Li Yuan, Pengfei Wan, and Di Zhang. Uniaa: A unified multi-modal image aesthetic assessment baseline and benchmark. *arXiv preprint arXiv:2404.09619*, 2024. [2](#), [3](#), [7](#), [8](#)

Fine-grained Image Aesthetic Assessment: Learning Discriminative Scores from Relative Ranks

Supplementary Material

8. FGAesthetics

In this section, we provide supplementary details on the construction of FGAesthetics, including: (1) detailed source distribution statistics, (2) implementation procedures of series refinement and rank calibration, and (3) prompt engineering methodology for comparative text generation.

8.1. Source Distribution of Data Collection

Tab. 6 presents the detailed source distribution of FGAesthetics. We collect 106,632 images from eight diverse sources spanning three distinct categories: natural images [5, 49], AI-generated content (AIGC) [9, 14, 20, 52], and cropping-based datasets [40, 50]. Through rigorous series refinement and rank calibration, the final dataset contains 32,217 images organized into 10,028 series, yielding an average of 4.47 pairs per series for fine-grained aesthetic discrimination. This diverse composition ensures that FGAesthetics encompasses comprehensive fine-grained aesthetic dimensions: natural photography quality, AI generation aesthetics, and compositional variations.

Table 6. Source Distribution and Statistics of FGAesthetics

Sources	Collected Img Count	After Series Refinement	After Rank Calibration	Series Count	Pair Count	Avg. Pairs per Series
SPS [5]	15,543	12,522	12,522	4,755	12,558	2.64
LSVQ [49]	2630	565	556	150	636	4.24
Pick-a-pic [20]	13,917	3,751	3,719	1,685	2,115	1.26
Q-Eval-100K [52]	11,430	418	372	180	196	1.09
Midjourney [14]	11,352	2,815	2,599	909	2,124	2.34
NIGHTS [9]	9,822	1,944	1,895	647	1,590	2.46
CPC [40]	29,348	8,485	8,480	1,310	21,242	16.22
GAIC [50]	12,590	2,088	2,074	392	4,402	11.23
Total	106,632	32,588	32,217	10,028	44,863	4.47

8.2. Details of Series Refinement

Metrics Filtering. Fig. 6 illustrates the detailed procedure of Metrics Filtering. We employ both generic and domain-specific measures to screen the data. First, generic measures compute the average SSIM and SIFT scores between each image and all others within its series. We then rank all images across the entire dataset and filter out the bottom 30% to exclude obvious outliers. For cropping series, we further calculate Intersection over Union (IoU) between crop frames and remove images with $\text{IoU} > 0.8$ (indistinguishable) or $\text{IoU} < 0.2$ (dissimilar). For AIGC series, we leverage original human-annotated T2I alignment scores to filter images severely misaligned with text prompts.

MLLMs Checking using Gemini. Given the robust contextual understanding capabilities of MLLMs, we also em-

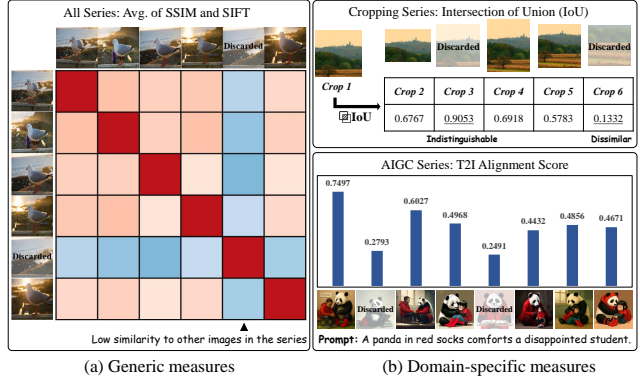


Figure 6. Detailed Procedure of Metrics Filtering. (a) Generic measures (average of SSIM and SIFT) exclude outliers within visually similar photo series. (b) Domain-specific measures (IoU for cropping series, T2I alignment scores for AIGC series) effectively identify nearly identical and dissimilar images.

ploy Gemini-2.5-pro [37] to validate the filtered series. This is achieved by presenting all images within a series to the model, guided by a carefully crafted prompt that requires a structured output for systematic parsing:

system: You are a rigorous image series filtering expert. Your task is to filter a given series of images and identify a subset that adheres to the specified criteria.

user: Your evaluation process is governed by the following criteria. Intra-group Similarity: Within the provided image series, identify the largest subset of images that are similar in theme, style, composition, and subject matter. They should appear as close variations of the same concept. If an image’s theme significantly deviates from the other images, it must not be included in the final similar group. Your output must be a formatted LIST: “selected_uids”: [“<uid.a>”, “<uid.b>”, ...].

Human Qualification. Following the automated filtering stages, comprehensive human qualification is implemented to ensure final data quality. All series undergo manual review by five human annotators via the annotation platform shown in Fig. 7. Samples that fail to meet fine-grained aesthetic criteria are discarded, ensuring that only high-quality series proceed to the aesthetic ranking annotation stage.

8.3. Details of Rank Calibration

Based on the refined data, we perform pairwise comparisons within each series to obtain global aesthetic rankings. Specifically, for a series of length n , a total of C_n^2 image pairs are generated. Each pair is evaluated by 10 trained an-

Table 7. Backbone ablation results on fine-grained and coarse-grained IAA tasks. For fine-grained evaluation on FGAesthetics, we report pair-level local discrimination using *Acc* and *F1*, and series-level ranking quality using *s-Acc* and *s-SRCC* across three source categories (Natural, AIGC, Cropping). *Pair* and *Series* represent category-averaged values of $(Acc+F1)/2$ and $(s-Acc+s-SRCC)/2$, respectively. For coarse-grained evaluation, we report SRCC and PLCC on AVA [26].

Backbone	Natural				AIGC				Cropping				Fine-grained		Coarse-grained	
	<i>Acc</i>	<i>F1</i>	<i>s-Acc</i>	<i>s-SRCC</i>	<i>Acc</i>	<i>F1</i>	<i>s-Acc</i>	<i>s-SRCC</i>	<i>Acc</i>	<i>F1</i>	<i>s-Acc</i>	<i>s-SRCC</i>	<i>Pair</i>	<i>Series</i>	SRCC	PLCC
ViT-B/16	0.779	0.779	0.753	0.729	0.709	0.707	0.561	0.482	0.774	0.773	0.488	0.590	0.753	0.600	0.770	0.781
ViT-B/32	0.711	0.711	0.634	0.503	0.653	0.651	0.445	0.301	0.740	0.740	0.491	0.548	0.701	0.487	0.747	0.760

Table 8. Out-of-Distribution generalization performance. OOD generalization is evaluated by training FGAesQ with one source category excluded and testing on fine-grained (all three categories) and coarse-grained (AVA [26]) benchmarks.

Backbone	Natural				AIGC				Cropping				Fine-grained		Coarse-grained	
	<i>Acc</i>	<i>F1</i>	<i>s-Acc</i>	<i>s-SRCC</i>	<i>Acc</i>	<i>F1</i>	<i>s-Acc</i>	<i>s-SRCC</i>	<i>Acc</i>	<i>F1</i>	<i>s-Acc</i>	<i>s-SRCC</i>	<i>Pair</i>	<i>Series</i>	SRCC	PLCC
FGAesQ	0.779	0.779	0.753	0.729	0.709	0.707	0.561	0.482	0.774	0.773	0.488	0.590	0.753	0.600	0.770	0.781
w/o Natural	0.745	0.745	0.710	0.630	0.704	0.703	0.569	0.455	0.771	0.771	0.488	0.583	0.740	0.573	0.770	0.782
w/o AIGC	0.767	0.766	0.720	0.675	0.687	0.685	0.542	0.425	0.765	0.765	0.482	0.577	0.739	0.570	0.776	0.786
w/o Cropping	0.765	0.764	0.727	0.678	0.699	0.698	0.552	0.438	0.755	0.755	0.462	0.558	0.739	0.569	0.772	0.783

```

impact.||By contrast, this one uses a much
tighter and more intimate focus, creating a
significantly more compelling narrative.",
    "prob_A_preferred": 0.167
}

```

Notably, the Comparison Direction of these two descriptions must be consistent with *prob_A_preferred*, that is, there cannot be a situation like *prob_A_preferred* is less than 0.5 but description A is more positive than description B.

To validate the quality of generated descriptions, we conduct a human evaluation. Three independent annotators assess 100 randomly sampled descriptions for plausibility, achieving an agreement rate of 93%. This confirms that our prompt engineering approach effectively generates meaningful and accurate explanations capturing fine-grained aesthetic differences. In Fig. 9, we further visualize the word cloud of MLLM-generated descriptions, where explicit comparative terms (e.g., “more”, “superior”, “less”) dominate the vocabulary.

9. FGAesQ

Following the implementation details and extensive experiments described in the paper, we present supplementary ablation studies to further validate the design choices of FGAesQ. Specifically, we investigate the impact of backbone architecture, Out-of-Distribution (OOD) generalization capability, and different DiffToken configurations.

9.1. Ablation of Backbone

We first investigate the impact of backbone architecture by replacing ViT-B/16 with ViT-B/32, a variant with a larger patch size. As shown in Tab. 7, ViT-B/16-based FGAesQ consistently outperforms ViT-B/32 across most fine-grained

and coarse-grained evaluations. The performance gap can be attributed to the smaller patch size (16×16 vs. 32×32) of ViT-B/16, which enables the model to capture more granular visual details. This is crucial for discerning subtle aesthetic differences required for both fine-grained ranking and coarse-grained scoring.

9.2. Out-of-Distribution (OOD) Generalization

We further conduct an Out-of-Distribution (OOD) generalization analysis of FGAesQ, as illustrated in Tab. 8. Specifically, we evaluate FGAesQ trained with one source category excluded and test its performance on both fine-grained and coarse-grained IAA tasks. The results reveal that performance degradation is most pronounced on the test set corresponding to the excluded training category. For instance, when trained without Natural data, the model shows the largest performance drop on Natural evaluation (from 0.779/0.753 to 0.745/0.710 for *Acc*/*s-Acc*), while maintaining relatively stable performance on AIGC and Cropping. This pattern holds consistently across all three categories, demonstrating the distinct nature of each data source. Coarse-grained performance remains largely stable across all training configurations, with SRCC and PLCC consistently above 0.77 and 0.78, respectively. Notably, excluding AIGC data even leads to a slight improvement in coarse-grained metrics, which can be attributed to the fact that AVA predominantly consists of natural images.

9.3. Ablation of DiffToken

As introduced in the main paper, the Difference-preserved Tokenization (DiffToken) module is governed by two key hyperparameters: the difference localization patch size and the percentile parameter p , which determines the proportion of aesthetics-decisive regions. We conduct an ablation

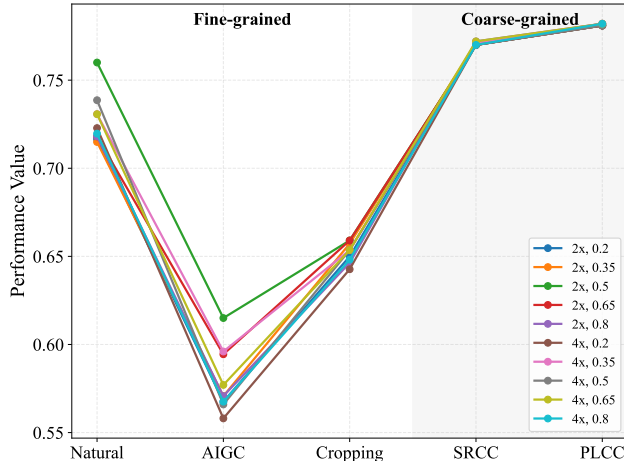


Figure 10. Ablation study on DiffToken configuration. Performance is evaluated across different difference localization patch sizes and percentile thresholds for identifying aesthetics-decisive regions. Fine-grained metrics show pair- and series-averaged performance across Natural, AIGC, and Cropping categories. Coarse-grained metrics report SRCC and PLCC on AVA [26].

study evaluating two patch sizes, 32×32 ($2 \times$ ViT patch size) and 64×64 ($4 \times$), combined with five percentile values: $p \in \{0.2, 0.35, 0.5, 0.65, 0.8\}$, as illustrated in Fig. 10.

The results yield several key insights. First, the optimal configuration is 32×32 with $p = 0.5$, achieving the best overall performance across all tasks. Second, performance exhibits a clear inverted-U pattern with respect to p , peaking around 0.5 and degrading at extremes. A small p (e.g., 0.2) fails to capture sufficient aesthetically-decisive regions, while too large p (e.g., 0.8) forces aggressive downsampling of non-decisive regions to meet the token constraints, losing critical global compositional information. Third, the finer 32×32 localization consistently outperforms 64×64 , as smaller patches more effectively detect subtle local variations crucial for fine-grained IAA. Finally, coarse-grained performance (SRCC/PLCC on AVA) remains stable across all configurations, confirming that DiffToken’s hyperparameters primarily affect fine-grained discrimination while having negligible impact on absolute aesthetic assessment.

10. Additional Visual Examples

In Fig. 11, we present additional visualization examples demonstrating FGAesQ’s fine-grained aesthetic discrimination capabilities. The visualizations showcase test series from Natural, AIGC, and Cropping categories, where FGAesQ consistently produces accurate rankings that closely align with human aesthetic judgments. Compared to state-of-art IAA methods (Charm [3], MUSIQ [17]), our approach exhibits superior sensitivity to subtle aesthetic variations, including lighting conditions, color

harmony, and compositional balance. This robust performance across different evaluation scenarios highlights FGAesQ’s versatility and practical value for real-world applications, such as photo album management and curation, text-to-image generation optimization, and automated composition refinement for photography enhancement.

11. Limitations

Dependency on Human Annotations. The reliance on extensive human annotations for fine-grained aesthetic discrimination poses scalability challenges and introduces potential subjective biases. Developing automated or semi-automated annotation strategies that maintain annotation quality while reducing human effort remains an important direction for future work.

Interpretability and Feedbacks. While FGAesQ achieves accurate fine-grained aesthetic discrimination, generating specific and actionable feedback to explain its predictions remains challenging. Developing methods that articulate precise aesthetic rationales, such as identifying compositional flaws or suggesting targeted improvements, would significantly enhance the practical applicability of fine-grained IAA models. This promising yet challenging direction merits further exploration.

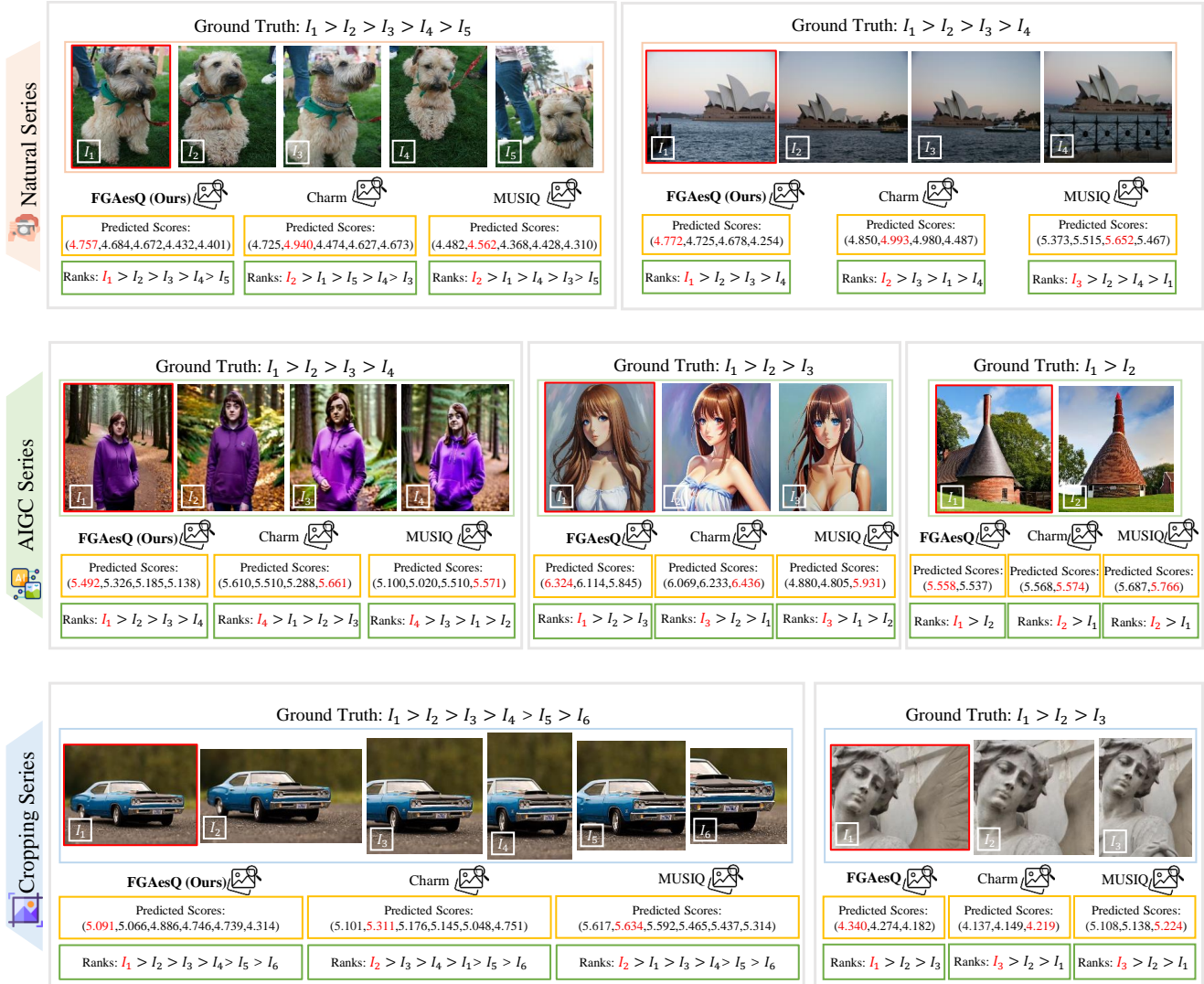


Figure 11. Additional visualization examples of FGAesQ on test series from Natural, AIGC, and Cropping categories.